Published for SISSA by Springer

Received: *April 15, 2022*
Accepted: *May 24, 2022*
Published: *June 29, 2022*

JHEP06(2022)165

Entanglement entropy and negativity in the Ising model with defects

David Rogerson,[a,1] **Frank Pollmann**[a,b] **and Ananda Roy**[c,1]

[a] *Department of Physics, T42, Technische Universität München, 85748 Garching, Germany*
[b] *Munich Center for Quantum Science and Technology (MCQST), 80799 Munich, Germany*
[c] *Department of Physics and Astronomy, Rutgers University, Piscataway, NJ 08854-8019 U.S.A.*

E-mail: david.rogerson@tum.de, frank.pollmann@tum.de, ananda.roy@physics.rutgers.edu

[1] Corresponding author.

https://doi.org/10.1007/JHEP06(2022)165

Abstract: Defects in two-dimensional conformal field theories (CFTs) contain signatures of their characteristics. In this work, we analyze entanglement properties of subsystems in the presence of energy and duality defects in the Ising CFT using the density matrix renormalization group (DMRG) technique. In particular, we compute the entanglement entropy (EE) and the entanglement negativity (EN) in the presence of defects. For the EE, we consider the cases when the defect lies within the subsystem and at the edge of the subsystem. We show that the EE for the duality defect exhibits fundamentally different characteristics compared to the energy defect due to the existence of localized and delocalized zero energy modes. Of special interest is the nontrivial 'finite-size correction' in the EE obtained recently using free fermion computations [1]. These corrections arise when the subsystem size is appreciable compared to the total system size and lead to a deviation from the usual logarithmic scaling characteristic of one-dimensional quantum-critical systems. Using matrix product states with open and infinite boundary conditions, we numerically demonstrate the disappearance of the zero mode contribution for finite subsystem sizes in the thermodynamic limit. Our results provide further support to the recent free fermion computations, but clearly contradict earlier analytical field theory calculations based on twisted torus partition functions. Subsequently, we compute the logarithm of the EN (log-EN) between two disjoint subsystems separated by a defect. We show that the log-EN scales logarithmically with the separation of the subsystems. However, the coefficient of this logarithmic scaling yields a continuously-varying effective central charge that is different from that obtained from analogous computations of the EE. The defects leave their fingerprints in the subleading term of the scaling of the log-EN. Furthermore, the log-EN receives similar 'finite size corrections' like the EE which leads to deviations from its characteristic logarithmic scaling.

Keywords: Anyons, Conformal Field Models in String Theory, Field Theories in Lower Dimensions, Lattice Integrable Models

ArXiv ePrint: 2204.03601

JHEP06(2022)165

Contents

JHEP06(2022)165

1 Introduction

Entanglement plays a central role in the development of long-range correlations in quantum critical phenomena. Thus, quantification of the entanglement in a quantum-critical system provides a way to characterize the universal properties of the critical point. For 1+1D quantum-critical systems described by conformal field theories (CFTs), entanglement measures provide a viable way to extract characteristics of the CFT. For instance, the von-Neumann entropy ($\mathcal{S}_A$) in the ground state [i.e., the entanglement entropy (EE)] for a subsystem (A) exhibits universal logarithmic scaling with the subsystem size [2, 3]. Here,

$$\mathcal{S}_A = -\mathrm{Tr}\rho_A \ln \rho_A, \;\; \rho_A = \mathrm{Tr}_B \rho, \tag{1.1}$$

where the total system with density matrix ρ is partitioned into A and B. The coefficient of this scaling determines a fundamental property of the CFT: the central charge, which quantifies, crudely speaking, the number of long-wavelength degrees of freedom. The aforementioned scaling, together with strong subadditivity property of entropy [4] and Lorentz invariance, leads to an alternate proof [5] of the celebrated c-theorem [6] in 1+1 dimensions. At the same time, the scaling of the EE in these gapless systems [7–9] and their gapped counterparts [10] lies at the heart of the success of numerical techniques like density matrix renormalization group (DMRG) [11, 12] in simulating 1+1D quantum systems.

Given the widespread success of the EE in characterizing bulk properties of quantum-critical points, it is natural to ask if the EE also captures signatures of boundaries in conformal-invariant systems [13]. For finite systems with boundaries at a conformal critical point, the EE receives a universal, subleading, boundary-dependent contribution, the so-called 'boundary entropy' [14, 15]. The latter, related to the 'ground-state degeneracy' of the system, plays a central role in a wide-range of problems both in condensed matter physics [16, 17] and in string theory [18]. The boundary contribution in the EE is a valuable diagnostic for identifying the different boundary fixed points of a given CFT [19–21]. In particular, the Ishibashi/Cardy states for the rational CFTs [22] lead to a direct computation of the different boundary entropies [13, 20].

Defects constitute the more general setting where one CFT, instead of being terminated with a given boundary condition, is glued to another CFT. Despite being ubiquitous, such defects are relatively less understood as far as their entanglement properties are concerned. A major difficulty is that lattice Hamiltonians for defects of rational CFTs are not yet available, although some progress has been made in this direction [23–25]. The notable exception is the free, real fermion (Ising) CFT, for which the defects have been completely classified and corresponding lattice Hamiltonians have been found [26–30]. Of particular interest are topological or purely transmissive defects. Such defects commute with the generators of conformal transformations [31–35] and thus, can be deformed without affecting the values of the correlation functions as long as they are not taken across field insertions (hence the moniker topological). They reflect the internal symmetries of the CFT and relate the order-disorder dualities of the CFT to the high-low temperature dualities of the corresponding off-critical model [33, 36, 37]. They also play an important role in the study of anyonic chains and in the correspondence between CFTs and three-dimensional topological field theories [38].

The importance of defects in the analysis of CFTs provides a natural motivation for the investigation of their entanglement properties. Consider the EE of a subsystem for two distinct geometries [see figure 1(a,b)]: i) where the defect is symmetrically located within the subsystem and ii) when the defect is located at the interface between the subsystem and the rest. For case i), as long as the defect sufficiently far from the edge of the subsystem, the leading order dependence of the EE (referred to as symmetric EE), is governed entirely by the bulk correlations around the edge of the subsystem. The subleading term depends on the defect. After usual folding maneuvers, the subleading term can be equated to a boundary entropy with double the bulk degrees of freedom [17, 29, 39]. This leads to predictions for the subleading term in the symmetric EE for defects in rational CFTs [40] when the size of the subsystem is much smaller than the system size. The situation for case ii) is more subtle. In particular, both the leading and subleading order terms of the EE (referred to as interface EE) depend on the defect. The leading order term has been computed using the replica trick for the free, compactified boson CFT [41] and the Ising CFT [42] (see also [43–45]). The coefficient of this leading order term defines an effective central charge that depends continuously on the defect strength. The subleading term, initially computed only for the topological defects [40, 42] using the corresponding twisted torus partition functions [31], was shown recently to be incorrect in ref. [1] for the Ising CFT using free-fermion computations.

JHEP06(2022)165

Figure 1. Geometric arrangements of the subsystem(s) and the rest of the system considered for the bipartite EE (a,b) and the log-EN (c) computations. The defect is indicated by a green dot. (a) Subsystem A is located symmetrically around the defect. (b) The defect lies at the interface between the subsystem (A) and the rest (B). (c) Two subsystems, B_1 and B_2, separated by a segment A, with the defect symmetrically located within A.

In this work, we analyze the entanglement properties of subsystems for the Ising CFT [1] with energy and duality defects using the density matrix renormalization group (DMRG) technique. The primary goals of this work are the following. First, DMRG provides a completely independent check of the free-fermion computations performed for the topological defect (a special case of the duality defect) in ref. [1]. Second, DMRG allows numerical computations to be performed in both finite and infinite systems by appropriately choosing boundary conditions (bcs) [12, 46]. As shown in ref. [1], the existence of a nonlocal zero mode in the topological case leads to nontrivial 'finite size corrections' [47] for both the symmetric and interface EEs. Here, we show that the same is also true for general duality defects away from the topological point [13]. Furthermore, by choosing infinite bc in our simulation, we explicitly verify that this correction disappears in the infinite system case. Third, we analyze the entanglement between two disjoint blocks, B_1 and B_2 separated by a segment containing a defect. Despite von-Neumann entropy's success in quantifying entanglement in CFTs, it does not quantify entanglement between subsystems when the total system (in this case $B_1 \cup B_2$) is in a mixed state, i.e., when $\mathrm{Tr}\rho^2 < 1$. To that end, we consider the logarithmic entanglement negativity (log-EN) [48] between the two blocks with the defect located symmetrically between them [see figure 1(c)]:

$$\mathcal{E}_{B_1,B_2} = \ln ||\rho^{T_{B_2}}|| = \ln \mathrm{Tr}|\rho^{T_{B_2}}|, \tag{1.2}$$

where $||\rho^{T_{B_2}}||$ is the trace-norm given by the sum of the absolute values of the eigenvalues of $\rho^{T_{B_2}}$. We compute the log-EN using DMRG. The latter allows us to compute the log-EN directly for the spin-system. This is important since the log-EN for a spin system is not, in general, the same as that of a fermionic model obtained after Jordan-Wigner (JW) transformation. This is because of the nonlocal nature of the JW transformation, where the fermionic degree of freedom in B_2 depends on the spin degrees of freedom in A (see, for instance, ref. [49] for quantification of this effect for the EEs of disjoint intervals). We show that the log-EN also exhibits logarithmic scaling as a function of the separation of the blocks for reasons similar to the case of the EE. We determine the coefficient of this scaling as well as the subleading term from our simulations. The former defines an effective central charge which depends continuously on the defect strength. While there are no analytical results available for the log-EN in the presence of defects, we verify that we recover the expected results for the leading order term in the different extremal cases, while providing

JHEP06(2022)165

numerical results for the rest. Interestingly, the effective central charge obtained from the log-EN scaling is different from that obtained from the interface EE computations. Similar to the EEs, the duality defect, due to the existence of zero energy modes, manifests itself through an offset in the log-EN, which we determine numerically. Finally, we address the question of finite size effects in the log-EN due to the nonlocal zero energy mode present in the duality defect. We show that similar to the EE, the nonlocal zero energy mode leads to nontrivial finite size corrections for the log-EN. These lead to deviations from the logarithmic scaling that is expected in systems without zero energy modes.

The paper is organized as follows. Section 2 summarizes the lattice Hamiltonians for the different defects of the Ising CFT. Section 3 describes the entanglement properties of the Ising model in the presence of defects. In section 3.1, we summarize the different scaling behaviors of the EE in the absence and presence of defects. This is followed by DMRG results of the symmetric and interface EE for open and infinite bcs (section 3.2.1 and section 3.2.2). Section 4 discusses the log-EN for two disjoint blocks separated by a defect. We summarize the scaling behavior of the log-EN in section 4.1, followed by DMRG results in section 4.2. Section 5 provides a concluding summary and outlook. We note that the symmetric EE and the log-EN, unlike the interface EE, do not follow immediately from the DMRG simulations. Additional computation is necessary to extract the relevant quantities. The technical details of this computation are summarized in appendix A.

2 Defects in the Ising CFT

In this section, we introduce the lattice Hamiltonians for the energy and duality defects in the Ising CFT for open and infinite bcs. The bcs are important since we are interested not only in the leading order scaling of the EE and EN, but also in the subleading terms.

The energy defect constitutes altering a ferromagnetic coupling of two adjacent spins. The resultant Hamiltonian is:

$$H_\epsilon = -\sum_{\substack{i=1\\ i\neq j}}^{L-1} \sigma_i^x \sigma_{i+1}^x - \sum_{i=1}^{L} \sigma_i^z - b_\epsilon \sigma_j^x \sigma_{j+1}^x, \tag{2.1}$$

where L is the length of the open chain and b_ϵ is the defect strength for a defect located between sites j and $j+1$. Note that one can also view the open bc as another energy defect inserted between sites L and 1 with zero defect strength. This model has been analyzed extensively in the past in the context of 2D classical Ising model with defect lines (see, for example, refs. [26–29, 50, 75, 80, 81]). The perturbing local defect term is marginal and gives rise to continuous scaling exponents [51, 52]. The Casimir term of the ground state energy depends continuously on the defect strength [26, 27]:

$$E_0(b_\epsilon) = -A_0 L - A_1(b_\epsilon) - \frac{A_2(b_\epsilon)}{L} + \ldots, \tag{2.2}$$

where $\ldots$ indicate subleading terms. Here, $A_0 = 4/\pi$ and

$$A_2(b_\epsilon) = \frac{\pi}{6} - 2\pi[F(b_\epsilon) - F(0)]^2, \;\; F(b_\epsilon) = \frac{1}{4} - \frac{1}{\pi}\tan^{-1} b_\epsilon. \tag{2.3}$$

JHEP06(2022)165

The explicit form of A_1 is not relevant for our purposes. For $b_\epsilon = 1$, we have a homogeneous chain with open bc. For this case, we recover the well-known result of $A_2(1) = \pi/24$ [recall that with the conventions of eq. (2.1), the velocity of light is 2]. An antiferromagnetic defect ($b_\epsilon = -1$) yields the same result since the defect can be removed by applying a unitary transformation on one half of the chain. This is possible because we are dealing with an open chain.[1] For more on the algebraic properties for the Ising chain with multiple defects, we refer the reader to refs. [26, 27, 53].

The duality defect consists of altering the ferromagnetic interaction of one bond to $b_\sigma \sigma_j^x \sigma_{j+1}^y$ where b_σ is the interaction strength. Equally important, there is no transverse field at the $j+1^{\text{th}}$ site. The Hamiltonian reads [29, 30]

$$H_\sigma = -\sum_{\substack{i=1\\ i\neq j}}^{L-1} \sigma_i^x \sigma_{i+1}^x - \sum_{\substack{i=1\\ i\neq j+1}}^{L} \sigma_i^z - b_\sigma \sigma_j^x \sigma_{j+1}^y. \tag{2.4}$$

The duality defect at $b_\sigma = 1$ is the topological defect in the Ising CFT.[2] The nontrivial nature of the duality defect is manifest in the fermionic language after a JW transformation [1] (see figure 2):

$$\gamma_{2k-1} = \sigma_k^x \prod_{j=1}^{k-1} \sigma_j^z, \gamma_{2k} = \sigma_k^y \prod_{j=1}^{k-1} \sigma_j^z, \tag{2.5}$$

where γ_j-s are real, Majorana fermion operators obeying $\{\gamma_j, \gamma_k\} = 2\delta_{j,k}$. In the fermionic language, the duality defect Hamiltonian is

$$H_\sigma^f = \frac{i}{2} \sum_{\substack{i=1\\ i\neq j}}^{L-1} \gamma_{2i}\gamma_{2i+1} + \frac{i}{2} \sum_{\substack{i=1\\ i\neq j+1}}^{L} \gamma_{2j-1}\gamma_{2j} + \frac{ib_\sigma}{2} \gamma_{2j}\gamma_{2j+2}. \tag{2.6}$$

The fermionic formulation also clarifies that the duality defect part of the Hamiltonian (the last term in the previous equation) is also a marginal perturbation and thus, gives rise to continuously varying scaling exponents. Note that the operator γ_{2j+1} does not occur in H_σ^f. It commutes with the Hamiltonian and anticommutes with the conserved $\mathbb{Z}_2$ charge Q:

$$[\gamma_{2j+1}, H_\sigma^f] = 0, \ \{\gamma_{2j+1}, Q\} = 0, \ Q = \prod_{i=1}^{L} (-i\gamma_{2j-1}\gamma_{2j}). \tag{2.7}$$

Thus, it is a zero-mode of the model which is perfectly localized in space. It has a partner zero-mode which is completely delocalized:

$$\Lambda(b_\sigma) = b_\sigma \sum_{k=1}^{j} \gamma_{2k-1} + \sum_{k=j+1}^{L} \gamma_{2k}. \tag{2.8}$$

[1] For a periodic ring with a single defect, $A_2(b_\epsilon) = \pi/6 - 2\pi F(b_\epsilon)^2$. In particular, for $b_\epsilon = 1$ (a periodic ring), we recover the standard result $A_2(1) = \pi/6$ and the expected central charge 1/2. On the other hand, for an antiperiodic chain, $A_2(-1) = -\pi/3$, yielding the effective central charge -1. [30].

[2] We use the duality defect Hamiltonian of refs. [1, 30], which is related by a local unitary rotation on the $j+1^{\text{th}}$ spin to the one considered in ref. [29].

JHEP06(2022)165

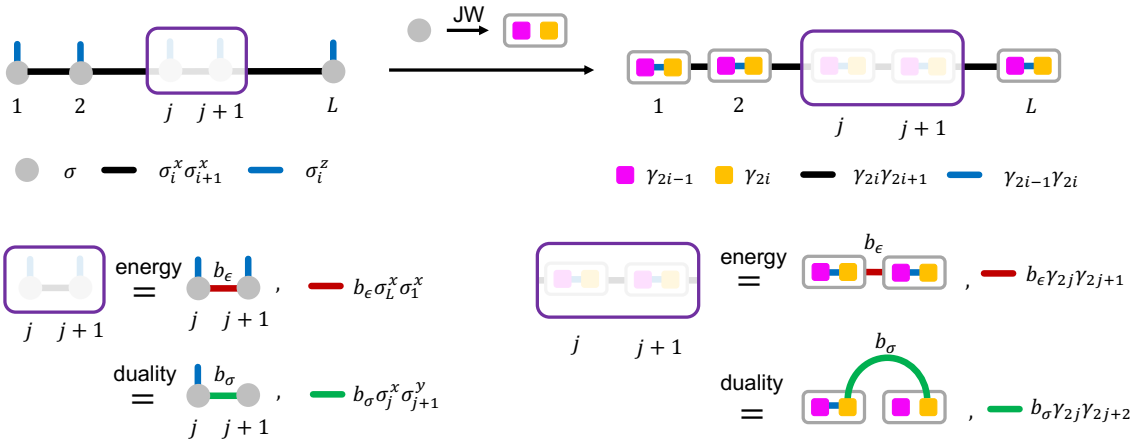

Figure 2. Schematic of the defect Hamiltonians in the spin and fermionic pictures. The JW transformation maps each spin to a pair of Majorana fermions [see eq. (2.5)]. The ferromagnetic couplings in the spin picture leads to couplings between Majorana fermions on neighboring sites (black links), while the transverse field corresponds to couplings between Majoranas within each site (blue links). The altered ferromagnetic coupling of the energy defect is indicated in maroon. The duality defect entails a $\sigma_j^x\sigma_{j+1}^y$ coupling indicated by a green bond, together with a missing transverse field on site $j+1$. In the fermionic picture, this leads to a Majorana zero mode (γ_{2j+1}). The other zero mode is delocalized throughout the system [see eq. (2.8)].

Note that the zero-modes exist for all values of b_σ and are not special features of the topological point. The fermionic Hamiltonian also reaffirms a CFT result [30]: H_σ^f describes a chain of $2L-1$ Majorana fermions or equivalently, $L-1/2$ spins. This is important for quantifying finite-size effects [1].

3 Entanglement entropies in the Ising CFT with defects

In this section, we briefly summarize the known properties of the EE in the Ising CFT for the two geometries considered in figure 1(a,b). First, we describe the logarithmic scaling of the EE in the absence of defects. Subsequently, we discuss the modifications of the aforementioned behavior of the EE due to the existence of defects. This is followed by a presentation of numerical results obtained using DMRG. All lengths are measured in units of the lattice spacing and are dimensionless.

3.1 Scaling of entanglement entropies

In the absence of defects, the behavior of the EE can be inferred from standard computations based on the replica trick [2, 3, 15]. For an infinite system, the EE for a subsystem of size l is given by

$$\mathcal{S}(l) = \frac{c+c}{6}\ln l + S_0 = \frac{c}{3}\ln l + S_0, \tag{3.1}$$

where $c = 1/2$ the central charge of the Ising model and S_0 is a nonuniversal constant. Here, in the first equality, we have explicitly shown that each edge of the subsystem (the entanglement cuts) contribute a factor of $c/6$ to the leading logarithmic dependence. For a

JHEP06(2022)165

finite system of length L, in the absence of zero-energy modes, the dependence is similar, with l replaced by the chord length $L\sin(\pi l/L)/\pi$ [3, 15]. The presence of the defect changes this dependence. This is explained below.

Consider first the case when the defect is *not* at the boundary between the subsystem and the rest (of an infinite system). For simplicity, we consider the case when the subsystem is located symmetrically around the defect, i.e., the case of the symmetric EE ($\mathcal{S}_{\rm S}$). In this case, the leading order logarithmic dependence is not altered. This is because the leading logarithmic contribution, which arises from the correlations around the entanglement cut, is *totally oblivious* of the defect. The defect strength could even be chosen such that the chain is cut into half without changing the leading logarithmic scaling. However, the subleading $\mathcal{O}(1)$ contribution contains information about the defect. This becomes apparent in the after folding the system at the defect, thereby transforming the defect problem to a boundary CFT one. Then, the subleading $\mathcal{O}(1)$ term can be equated to a boundary entropy with double the bulk degrees of freedom [17, 29, 39]. The resulting expression is

$$\mathcal{S}_{\rm S}(l) = \frac{c}{3}\ln l + \tilde{S}_0, \tag{3.2}$$

where we have indicated the modified subleading expression by $\tilde{S}_0$. For a finite-size system, as for without any defects, the scaling behavior is obtained by replacing the subsystem-length by the chord-length.

Now, consider the case when the defect lies exactly at one of the edges of the subsystem, i.e., the case of the interface EE. The other end of the subsystem is somewhere in the bulk of the total system. It turns out that for the Ising CFT with defects, the interface EE, also exhibits a logarithmic scaling. But, both the leading order logarithmic scaling and the subleading $\mathcal{O}(1)$ terms are modified:

$$\mathcal{S}_{\rm I}(l) = \frac{c_{\rm eff}+c}{6}\ln l + S_0', \tag{3.3}$$

where $c_{\rm eff}$ is an effective central charge that depends continuously on the defect strength with $c_{\rm eff} \leq c$. Note that this equation is valid for an infinite total system size. The coefficients of the logarithm, $c_{\rm eff}$ and c, arise from the entanglement cuts at the defect and the other end of the subsystem respectively. This logarithmic scaling and the continuous dependence of $c_{\rm eff}$ on the defect strength is a non-generic scenario that arises due to the fact that the defect terms in the Hamiltonian are marginal perturbations, which gives rise to continuous scaling exponents. It is also worth noting that the effective central charge is merely the coefficient of the logarithmic scaling and bears little algebraic significance. Importantly, $c_{\rm eff}$ is different from the central charge obtained from the ground state energy dependence (see section 2). Note also that the subleading term, S_0', is also different compared to the case without defects. For a finite total system of length L, often one can consider the interface EE between the left and right halves of the system. Then, the interface EE is

$$\mathcal{S}_{\rm I}(L) = \frac{c_{\rm eff}}{6}\ln L + S_0''. \tag{3.4}$$

JHEP06(2022)165

Note that there is no factor of c in the coefficient arising from the second entanglement cut, which now coincides with the physical boundary of the system. Also, the subleading term is different compared to eq. (3.3) since now it depends explicitly on the bcs of the system.[3]

In this way, both the symmetric and interface EEs serve as viable diagnostics for detection of defects. The case of the interface EE is particularly interesting since there is no simple folding maneuver that converts the defect problem to a boundary CFT one. Clearly, in the absence of a defect, the $c_{\text{eff}} = c$, which can be viewed as a manifestation of perfect transmission of modes carrying information. In the presence of a defect, reflection of these information-carrying modes causes c_{eff} to be less than c. However, there exist nontrivial defects, which still leave $c_{\text{eff}} = c$. Topological defects are precisely such perfectly-transmissive defects, which leave their fingerprints only in the subleading term, S_0' or S_0'', in the interface EE (see section 3.2).

The preceding discussion about the logarithmic dependence of the symmetric and interface EEs is applicable only in the absence of zero energy modes. Defects in the Ising CFT can give rise to both local and nonlocal zero energy modes: e.g., the critical Ising chain with antiperiodic bc [54] and the Ising CFT with duality defects (see section 2). In the computation of ground-state properties, one can consider the case when the zero energy modes are filled or empty. The system could also be considered in a statistical mixture of the filled and empty states. The purity of the system has nontrivial consequences on the entanglement properties of its subsystems [47, 55]. For Hamiltonians with zero energy modes, the logarithmic dependence of the EE is valid, in general, only in the limit when subsystem size is infinitesimal compared to the system size. When the subsystem occupies a finite fraction of the system, the nonlocal zero energy modes give rise to nontrivial finite size corrections [1, 47]. The latter are particularly important for the interface EEs between the left and right halves of the system, where the subsystem is necessarily a finite fraction of the total system. Next, we consider the case when the total state of the system is pure (see ref. [1] for results when the total system is mixed) and present numerical results for the symmetric and interface EEs.

3.2 DMRG results

Here, we consider the various defect Hamiltonians of section 2 and compute the EEs for different subsystems using DMRG. The DMRG simulations were performed using the TeNPy package [46]. We consider two cases: i) where the size of the total system is infinite and ii) when the size of the total system is finite with open bcs at the ends. We consider these two different cases to explicitly demonstrate the influence of the non-local zero mode for the topological defect of the Ising CFT. For technical details of the computation, see appendix A.

[3] In the absence of a defect, the EE between the left (of length l) and the right (of length $L-l$) parts of the system is given by [3, 15]: $\mathcal{S}(l) = \frac{c}{6} \ln\left(\frac{2L}{\pi} \sin\frac{\pi l}{L}\right) + \ldots$, where the dots indicate the subleading contributions. In the absence of the defect, eq. (3.4) is a special case: $l = L/2$. However, in the presence of a defect, only the interface EE between left and right halves is known for finite systems.

JHEP06(2022)165

3.2.1 Symmetric entanglement entropy

Consider the EE of a subsystem located symmetrically around the energy defect for an infinite system (left panel of figure 3). The DMRG simulations were performed using the single-site DMRG algorithm for different defect strengths b_ϵ. The maximum bond dimension (χ) used was 100. While the ground state can be obtained, in general, for much larger values of χ, the computation of the symmetric EE (and the log-EN performed later) scales as χ^4 and thus, prevents us from using larger values of χ. However, as shown below, this low bond-dimension is already sufficient to capture the universal properties of the model. The state was obtained by converging the relative ground state energy to 10^{-11} for and the average von-Neumann entropy up to 10^{-8} for the chosen $\chi = 100$. Recall that $b_\epsilon = +1$ corresponds a homogeneous infinite chain without any defect. For both the energy defects of different strengths, as expected from eq. (3.2), the symmetric EE scales with $\ln l$, l being the system size with a coefficient $c/3$, where $c = 1/2$. The subleading term $\tilde{S}_0$, consisting of universal and non-universal parts, is also independent of the defect strength b_ϵ. In the folded picture, the universal part corresponds to the same boundary entropy due to the same g-function ($= 1$) [29, 56]. The specific case of $b_\epsilon = -1$ can be verified explicitly since the defect can be removed by a unitary transformation on one half of the infinite chain. Similar computations were done for the finite system (right panel of figure 3). The results are identical after substituting the $l \to L \sin(\pi l/L)/(\pi)$.

The duality defect on the other hand shows dramatically different behavior. As expected, the leading logarithmic scaling is identical to the case of the energy defect for the same reasoning. However, the subleading term, $\tilde{S}_0$, is different. For *all* subsystem sizes in an infinite system and for subsystem sizes $l \ll L$ in the finite system,

$$\tilde{S}_0 = S_0 + \frac{1}{2}\ln 2 \tag{3.5}$$

This result is true for all strengths, (b_σ), of the duality defect and not just the topological point: $b_\sigma = 1$. Note that only the difference between $\tilde{S}_0$ and S_0 is universal. Physically, this extra contribution arises due the presence of the *localized* unpaired Majorana zero mode localized within the subsystem [see eq. (2.7)]. In the folded picture, this defect corresponds to the 'continuous Neumann boundary fixed point' [29], with a g-function $= \sqrt{2}$. The difference in the symmetric EEs between the duality and the energy defects is given precisely by difference of the logarithm of the two g-functions. As shown in figure 3 (right panel), for a finite system size L, when subsystem occupies an appreciable fraction of the total system, the symmetric EE no longer exhibits the usual logarithmic scaling. This is because of the delocalized Majorana zero mode [see eq. (2.8)] present in the system. The complete functional dependence of the subleading term is [1]:

$$\tilde{S}_0 = S_0 + \frac{1}{2}\Delta S\left(1 - \frac{l}{L}\right), \tag{3.6}$$

where [47]

$$\Delta S\left(\frac{l}{L}\right) = \frac{\pi l}{L}\int_0^\infty dh \tanh\left(\frac{\pi l h}{L}\right)[\coth(\pi h) - 1], \tag{3.7}$$

JHEP06(2022)165

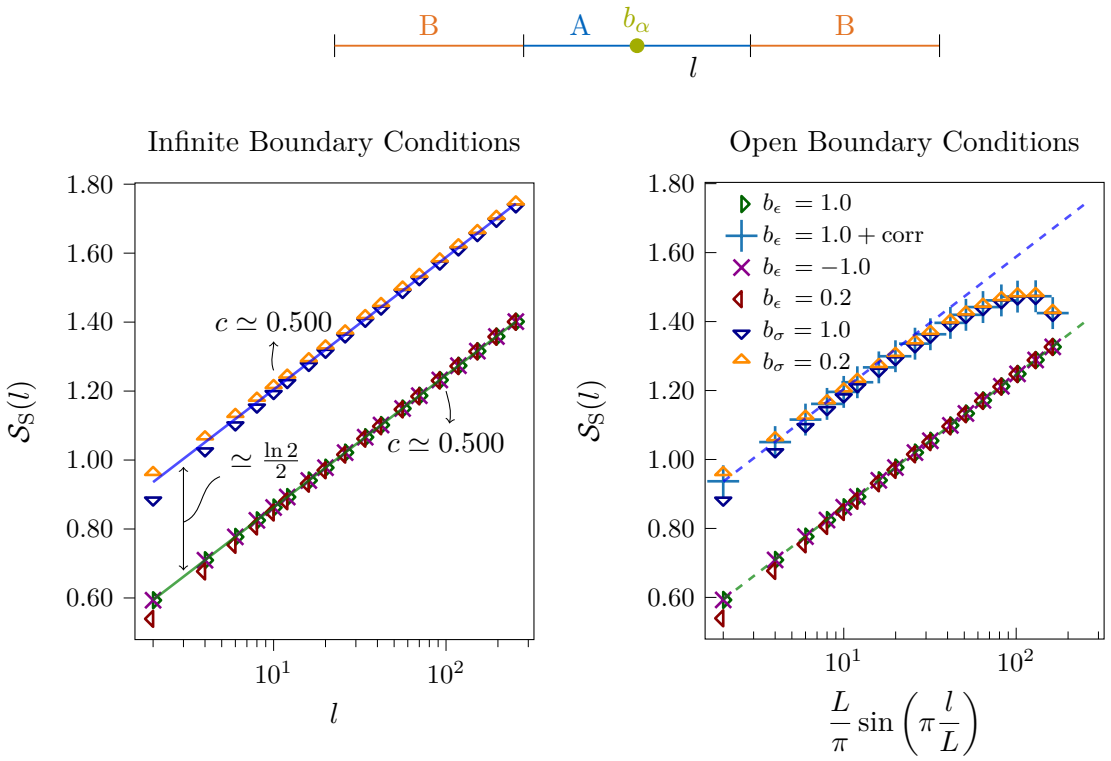

Figure 3. Scaling of the symmetric EE, $\mathcal{S}_S(l)$, for a segment A of length l located symmetrically around a defect. We show the results for infinite (left) and open (right) bcs. For finite bc, the total system length is denoted by L. (Left) The symmetric EE scales logarithmically with l for both energy and duality defects for all defect strengths [see eq. (3.2)]. The coefficient of the logarithm for every case gives the expected central charge $c = 1/2$ (the errors in the fits occur in the fourth decimal places). Recall that this coefficient is sensitive to correlations around the entanglement cut, which in this case is located far from the defect (see discussions in section 3.1). The subleading is sensitive to the defect type. For the duality defect of a given strength, this subleading term is $(\ln 2)/2$ higher than the energy defect of the corresponding strength. This can be viewed as a consequence of the zero-energy mode localized at the defect [see eq. (2.7)]. We note that the symmetric EE does not seem to depend, at least up to $\mathcal{O}(1)$ corrections, to the actual defect strength value for a given defect class. (Right) For finite systems, the results are similar to the infinite case for $l \ll L$ with the subsystem size replaced by the chord-length. As l is increased to values comparable to L, deviations occur from usual logarithmic scaling for the duality defect cases due to the existence of the delocalized zero-energy mode [see eq. (2.8)]. The predicted values of the duality defect cases are indicated by the blue crosses, which are obtained by adding $\Delta S(1 - l/L)/2$ to the symmetric EE without any defect.

Note that $l/L \ll 1$, $\Delta S \sim \pi^2 l^2/12L^2$, while $\Delta S(1) = \ln 2$. This nontrivial expression for the EE was first computed for an antiperiodic Ising chain in ref. [47]. In contrast to the latter problem, which had *two* nonlocal zero modes, the Ising model with duality defects contains one local and *one* nonlocal zero mode. This accounts for the factor of 1/2 difference between our result and those obtained in ref. [47].

JHEP06(2022)165

3.2.2 Interface entanglement entropy

Next, we investigate the scaling of the interface EE. We compute the EE for different bipartionings of an infinite system and a finite system with open bc. The defect is located at the center of the system and thus, one specific choice of partitioning yields the interface EE for the model. For the scaling analysis, we consider only the interface EE between the left and right halves of the infinite/finite system. In this case, for a finite system, the scaling behavior of the interface EE is given eq. (3.4). For an infinite system, the scaling is more nontrivial. In principle, for the infinite system in the presence of defects, the correlation length is still infinite (recall that the defect perturbations are marginal perturbations of the Ising CFT). However, in an actual DMRG simulation of an infinite system, the correlation length is rendered finite due to 'finite entanglement truncation' [8, 9]. The entanglement truncation is a direct consequence of the finite number of Schmidt states kept during the numerical simulation. The resulting finite correlation length provides a natural length-scale for the scaling of the interface EE. In the absence of defects, this scaling is analogous to the finite-size scaling, with the system size being replaced by the computed finite correlation length in eq. (3.4). In this work, we show that the scaling obtained due to finite entanglement truncation works (surprisingly well) for the case with defects, with the correlation length computed for the system without defects keeping the entanglement truncation the same. We also note that this issue arises only for the scaling of the interface EE between left and right halves of an infinite system. In the other cases, the block size provides the relevant length-scale for scaling (see section 3.1).

First, consider the energy defect. For $b_\epsilon = \pm 1$, the EEs are identical and constant for different bipartitionings for an infinite system. That they are identical and constant is because the system is translation-invariant (recall that the Hamiltonian for $b_\epsilon = -1$ can be reduced to that for $b_\epsilon = 1$ by a unitary transformation). For $b_\epsilon = 0.2$, the EE is similar to the case without defects sufficiently far away from the defect (left panel of figure 4). However, as the defect is approached, the EE dips below the value obtained without defects. This entanglement dip is due to the reflections of entanglement carrying modes at the defect. For finite systems, similar results arise with the important distinction that in absence of the defect, the EE is not a constant value, but rather obeys a logarithmic dependence with subsystem size (see footnote 3). As for the infinite case, introduction of a defect leads to a dip in the EE for partitionings of the system close to the defect bond. In the presence of defects, the explicit form of the dependence of the EE for arbitrary bipartionings is not known. However, the interface EE (when the bipartioning is done by cutting the system at the defect bond) exhibits the predicted logarithmic scaling with the total system size (correlation length) for finite (infinite) systems [see eq. (3.4) and figure 5]. The central charge obtained is close to the predicted value [42–45]:

$$c_{\text{eff}}(s) = \frac{s}{6} - \frac{1}{6} - \frac{1}{\pi^2}\Big[(s+1)\ln(s+1)\ln s + (s-1)\text{Li}_2(1-s) + (s+1)\text{Li}_2(-s)\Big], \quad (3.8)$$

where $s = |\sin(2\phi_0)|$ and Li_2 is the dilogarithm function [57] and $b_\epsilon = \cot\phi_0$. The complete dependence of the effective central charge and the analytical predictions are shown in the left panel of figure 7. The offset, S_0'', for different defect strengths is plotted in the top right

JHEP06(2022)165

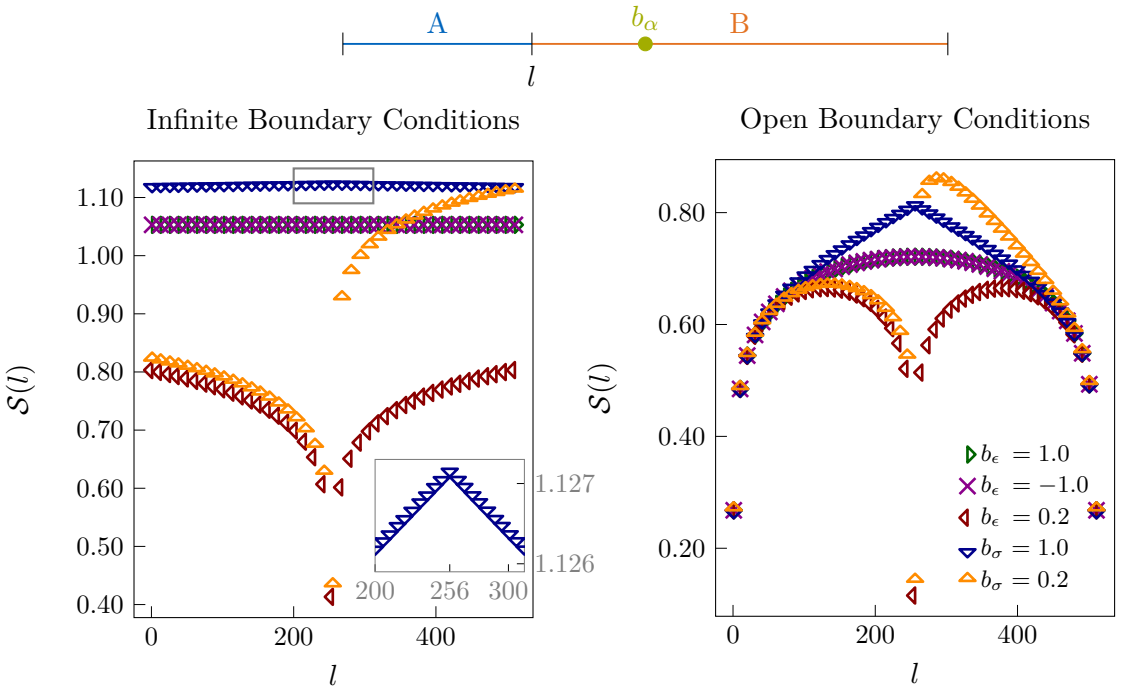

Figure 4. The EE, $\mathcal{S}$, for different bipartionings of the system for infinite (left) and open (right) bcs obtained by the DMRG calculation for energy and duality defects for $\chi = 100$. In the middle of the system is an energy ϵ-defect or a duality σ-defect of various strength. As for the symmetric EE, the results for the $b_\epsilon = \pm 1$ are identical. For the latter, in the infinite system case, the result is a constant EE for different bipartitionings. The actual value of this constant depends on the amount of entanglement truncation [8, 9] and will be different for different values of χ. The corresponding results for the finite system follow the dependence given in footnote 3. For defect strengths $b_{\epsilon,\sigma} < 1$, the EE exhibits a dip centered at the defect-bond due to the reflections of the entanglement-carrying modes at the defect. On the other hand, the EE is discontinuous for the duality defect with $b_\sigma < 1$ as the defect is traversed. This is a consequence of the zero energy mode localized at the defect. The situation is different for the topological defect: $b_\sigma = 1$, which is associated with a *higher* interface EE compared to $b_\epsilon = 1$ (see inset of the left panel for infinite and right panel for finite system results). The scaling of the interface EE with correlation length (system size) for infinite (finite) systems is shown in figure 5.

panel of figure 7. We are not aware of any analytical predictions for the universal part, if any, of this offset for the energy defect.

Now, consider the duality defect away from the topological point ($b_\sigma \neq 1$). As expected, sufficiently far away from the defect, the EEs approach the case without defects. As the defect location is approached from the left, the EE goes down as in the energy defect. However, upon crossing the duality defect, the EE exhibits a discontinuous jump (see figure 4). This is due to the localized zero mode that is included in the subsystem (see figure 2 and surrounding discussions). Despite this discontinuous behavior, for partioning at the defect bond, the interface EE exhibits a logarithmic scaling with an effective central charge which is identical to the energy defect case [eq. (3.8)]. We see that the offset computed for the duality defect is *different* from that obtained for the energy defect for a

JHEP06(2022)165

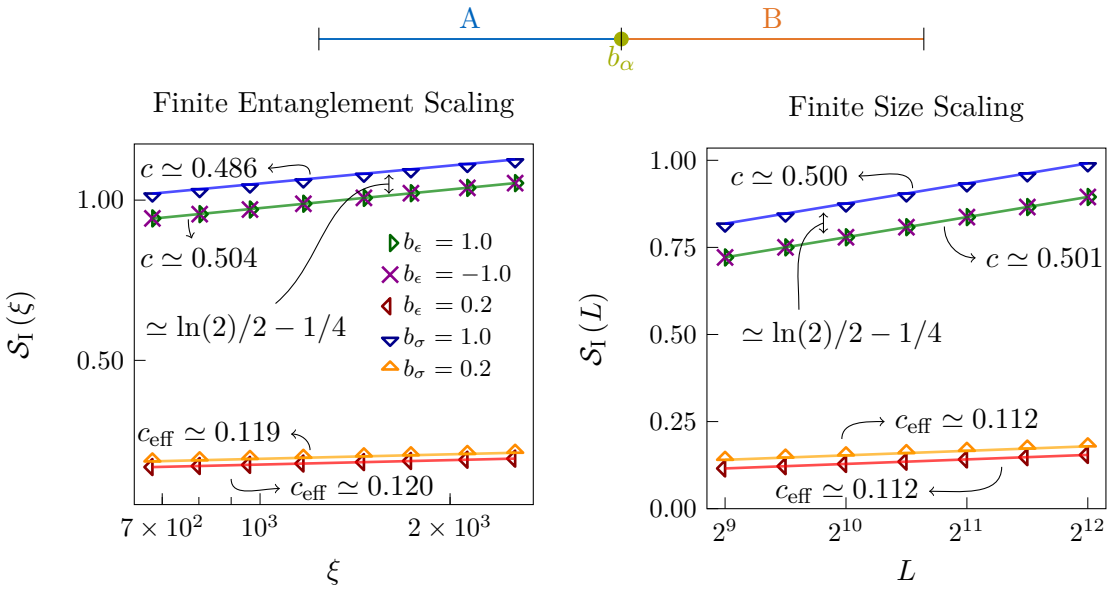

Figure 5. Scaling of the interface EE, S_{I}, with correlation length (ξ) and system size (L) for infinite (left panel) and open (right panel) bcs. For the infinite bc, the bond dimension (χ) was increased from 50 to 100 to increase the correlation length. For both bcs, the $b_\epsilon = \pm 1$ and $b_\sigma = 1$, the coefficient of the logarithmic scaling [see eq. (3.3), with $L \to \xi$ for infinite bc] gives a central charge of $c \simeq 0.5$. The same for $b_{\epsilon,\sigma} = 0.2$ leads to an effective central charge $c_{\text{eff}} \simeq 0.112$, in agreement with see eq. (3.8). The fit errors obtained are in the fourth decimal places. We notice that the infinite system scaling results are slightly worse than the finite system. We believe this is due to the fact that the correlation length computed for the translation-invariant system is close, but not the same as the system with defects. Fitting to eq. (3.3), with $L \to \xi$ for infinite bc, we compute the offsets, S_0'' for the different defects. The full dependence of the offsets on the defects is shown in figure 7. In particular, the obtained difference between the $b_\sigma = 1.0$ and $b_\epsilon = 1.0$ cases equals $\ln(2)/2 - 1/4$ up to second digit of precision. This is in agreement with eq. (3.9) for both infinite and open bcs and compatible with the result obtained for periodic bcs in ref. [1].

given defect strength. However, we are not aware of an analytical prediction for the offset for $b_\sigma \neq 1$. Only for the topological case are both the effective central charge and the offset analytically predictable [1]. This is discussed next.

The topological point corresponds to the case when the interface EE satisfies eq. (3.4) with $c_{\text{eff}} = c = 1/2$ (see section 3.1), which is indicative of the perfect transmission of information across the defect. The results for this case are shown in figure 4. As the non-topological case, the EE for partitioning the system far from the defect is close to the results obtained for without any defect. However, as the subsystem size increases, the deviation from the no-defect case becomes apparent. Unlike the non-topological case, the dip in the EE is replaced by a peak that is *higher* than the EE curve for the case without defects. That there is no dip is due to the perfect transmission of information. That the interface EE is even higher than the no-defect case is due to the presence of the zero energy modes in the system. The scaling of the interface EE with the correlation length (system size) for infinite (open) bc reveals that the offset S_0'' is larger than that obtained for the

JHEP06(2022)165

no-defect case by:

$$\Delta S_0'' = S_0''(b_\sigma = 1) - S_0''(b_\epsilon = 1) = \frac{1}{2}\Delta S\left(\frac{1}{2}\right) = -\frac{1}{4} + \frac{1}{2}\ln 2, \tag{3.9}$$

where ΔS is defined in eq. (3.7). As pointed out in ref. [1], this offset occurs entirely due to a 'finite-size effect' correction arising due to the existence of nonlocal zero-modes. This finite size effect is unavoidable since the interface EE here is computed between left and right halves of the system, i.e., between subsystem and the rest each being of size $L/2$. Importantly, this *positive* offset bears no relationship to the specific modular S-matrix elements and the claimed offset of $-\ln 2$ predicted in refs. [40, 42]. The source of the discrepancy can be traced back to the fact that the twisted torus partition functions do not faithfully capture the geometric setup of the interface EE computation. It is worth emphasizing that this discrepancy plagues *only* the subleading/boundary term of the interface EE and not the logarithmic/bulk scaling for all values of b_σ. This is why the effective central charge is consistent with the field theory computations [see eq. (3.8)], but not the subleading term. For more details regarding subtle finite size effects in the topological case, we refer the reader to ref. [1].

To summarize, in this section, we have computed the symmetric and interface EEs for the Ising CFT with energy and duality defects. The two computed EEs quantify the entanglement between the subsystem and the rest when the defect is located symmetrically within and at the edge of the subsystem respectively. However, the two computed EEs are measures of entanglement only when the total system is in a pure state. In the next section, we analyze the role of defects in entanglement between subsystems when they together are in a mixed state.

4 Entanglement negativity in the Ising CFT with defects

Here, we compute the entanglement between two disjoint subsystems, B_1 and B_2, separated by a segment of size l, with the defect located symmetrically within A [see figure 1(c)]. In this case, the von-Neumann entropy does not quantify the entanglement between B_1 and B_2 since the state of $B_1 \cup B_2$ is mixed, even though $A \cup B_1 \cup B_2$ is in a pure state [58, 59]. Measures quantifying mixed state entanglement are nontrivial to compute for many-body systems. A well-known exception is the log-EN [48] [see eq. (1.2)]. The latter has been computed analytically for CFTs using the replica technique [60–62] and has been shown to reveal certain characteristics of the CFTs. The EN computations have since been generalized to other systems: massive deformations of CFTs [63], non-equilibrium systems [64, 65] and Kondo spin chains [76–78] to name a few.

As we show here, the log-EN finds a natural application in quantifying entanglement between the subsystems in the configuration described in figure 1(c). Thus far, to the best of our knowledge, the log-EN has never been computed for defect CFTs analytically or numerically. Here, we compute the log-EN using DMRG. As shown in appendix A, the computation of the log-EN is as resource-consuming as that of the symmetric EE. Yet, as shown below, in the presence of defects, the log-EN shows dramatically different results

JHEP06(2022)165

compared to the symmetric EE. Before presenting our numerical results, we summarize the expected scaling behavior of the log-EN.

4.1 Scaling of entanglement negativity

Consider first the case without any defect. It is known that for certain configurations of subsystems, the log-EN exhibits logarithmic scaling behavior similar to the EE. In fact, for $A = \emptyset$ in figure 1(c), the log-EN reduces to the Renyi entropy with Renyi index $n = 1/2$ [60]. The latter exhibits the characteristic logarithmic scaling of EEs with the system size. The situation is more complex when A has a finite extent. In particular, it can be shown that without a defect, for two disjoint semi-infinite intervals, B_1, B_2, the log-EN scales as

$$\mathcal{E}(l) = -\frac{c}{4} \ln l + \mathcal{E}_0, \tag{4.1}$$

where l, the size of the segment A, is the separation between B_1 and B_2 and $\mathcal{E}_0$ is a non-universal constant. Note the *negative* sign in front of the logarithm. It is useful to contrast this setup with the symmetric EE setup of figure 1(a). The symmetric EE scales also logarithmically with the size of the segment A, but with a coefficient $+c/3$ [see eq. (3.1)]. Importantly, the symmetric EE quantifies the entanglement between A and $B_1 \cup B_2$ and *not* between B_1 and B_2.

Now, consider the case when there are defects. Unlike the symmetric EE, the log-EN contains signatures of the defect both in the leading logarithmic scaling and the subleading terms. As we numerically demonstrate below, the defects, being marginal perturbations, lead to a continuously varying central charge in the scaling of the log-EN:

$$\mathcal{E}(l) = -\frac{\tilde{c}_{\text{eff}}}{4} \ln l + \tilde{\mathcal{E}}_0, \tag{4.2}$$

where $\tilde{c}_{\text{eff}}$ depends on the defect strength [compare eq. (3.2)]. In particular, for perfectly reflective ($b_{\epsilon,\sigma} = 0$) and perfectly transmissive ($b_{\epsilon,\sigma} = 1$) defects, $\tilde{c}_{\text{eff}} = 0$ and $1/2$ respectively. This is indicative of the expected zero and maximal entanglement between the blocks B_1 and B_2. In between these two points, $\tilde{c}_{\text{eff}}$ grows monotonically. We emphasize that except for the two special points, $\tilde{c}_{\text{eff}} \neq c_{\text{eff}}$, the latter being the effective central charge obtained for the interface EE [see eq. (3.8)]. This difference can be traced to the partial transposition in the definition of the EN. The subleading term, $\tilde{\mathcal{E}}_0$, also contains information about the defects, similar to $\tilde{S}_0$ and S_0'' for the symmetric and interface EEs. Note that eq. (4.1) is valid only when the two blocks B_1 and B_2 are both semi-infinite. For finite-size systems, we find an analogous scaling with the usual substitution of l by $L \sin(\pi l/L)/\pi$, where L is the total system-size.

We are not aware of any analytical computation of $\tilde{c}_{\text{eff}}$ and $\tilde{\mathcal{E}}_0$ in the presence of defects. In the following section, we present numerical results obtained using DMRG. As shown below, the zero energy modes associated with the duality defect (see section 2) also lead to nontrivial finite-size corrections that lead to deviation from the logarithmic scaling given in eq. (4.2) for the log-EN. We exhibit this explicitly by performing the DMRG simulations with infinite and open bcs.

JHEP06(2022)165

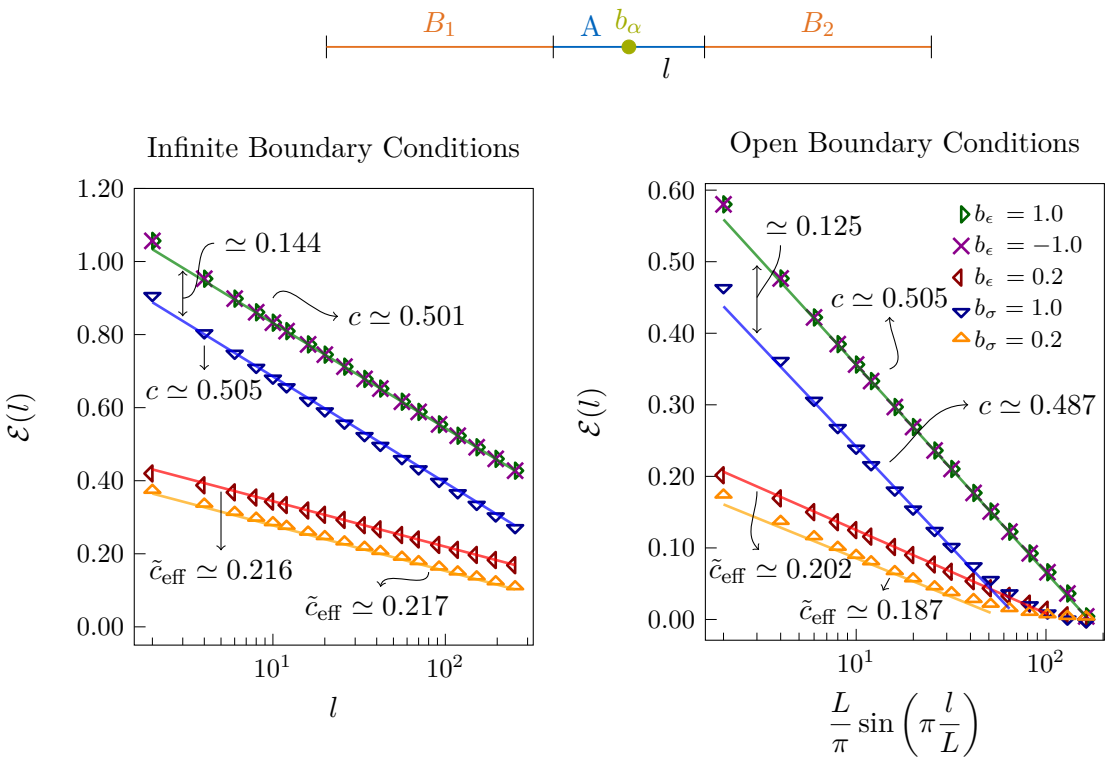

Figure 6. Scaling of the log-EN, $\mathcal{E}$, for infinite (left) and open (right) bcs. With increasing separation, l, the entanglement between B_1 and B_2 decreases logarithmically [see eq. (4.2)], as is expected from the intuition that correlation function of the degrees of freedom in B_1 and B_2 diminishes algebraically. The effective central charges, $\tilde{c}_{\text{eff}}$, obtained from the scaling of the log-EN is different from that obtained from the scaling of the interface EE. The fit errors obtained are in the fourth decimal places. Note also that the offset for the duality defects are *smaller* than those for the energy defects of corresponding strengths. This is in contrast to the corresponding results for the interface EE (see figure 5 and maintext for further discussion). For the duality defect results with open bc, as for the interface EE, the presence of zero energy modes leads to deviations from the logarithmic scaling of the log-EN. This leads to poorer estimates of the effective central charges for the open bc case compared to the infinite case.

4.2 DMRG results

The log-EN is computed from the ground state obtained using DMRG (see appendix A for technical details). Figure 6 shows the results for the energy and the duality defects. As expected, the results are identical for $b_\epsilon = \pm 1$ (see section 3.2 for similar results for the EE), with $\tilde{c}_{\text{eff}} = 1/2$ (see figure 7). Lowering the defect strength leads to a monotonically decreasing $\tilde{c}_{\text{eff}}$ culminating in $\tilde{c}_{\text{eff}} = 0$ for zero defect strength, when the 1D system is cut into half and there is zero entanglement between B_1 and B_2. As is evident from figure 7, $\tilde{c}_{\text{eff}} \geq c_{\text{eff}}$ with equality being satisfied only for perfectly reflective and perfectly transmissive defects. When the size of $A \cup B_1 \cup B_2$ is finite (say L), the scaling is similar after the substitution of l by $L \sin(\pi l/L)/\pi$.

JHEP06(2022)165

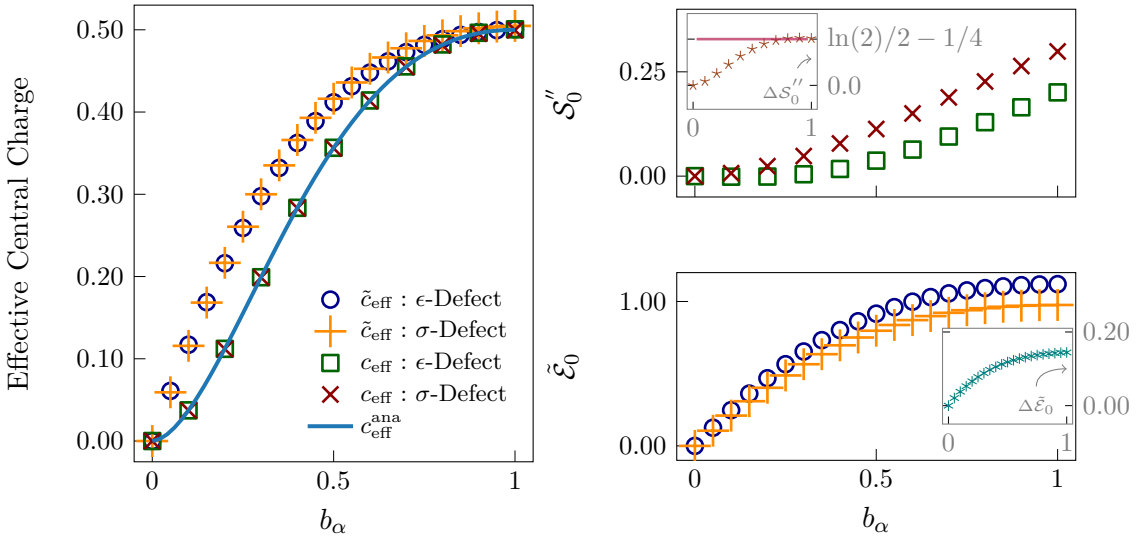

Figure 7. Variation of the effective central charges (left) and the sub-leading corrections (right) with the defect strength for the energy and duality defects. The effective central charges, $c_{\rm eff}$, obtained from the scaling of the interface EE, $\mathcal{S}_{\rm I}$, for the energy and duality defects are identical for a given defect strength and are compatible with the predictions of eq. (3.8), denoted in this plot by $c_{\rm eff}^{\rm ana}$. The computed values $\tilde{c}_{\rm eff}$ from the log-EN again agree in between the defects of equal strength. The subleading corrections on the right increase with their difference (shown in the respective inserts) eventually saturating towards a fixed value. For the interface EE, this offset $\Delta\mathcal{S}_0''$ is in good agreement with the analytic prediction for $b_\sigma = 1$ of eq. (3.9), shown as the pink line. The corresponding subleading corrections for the log-EN are shown in the bottom right panel.

The duality defect for the corresponding defect strengths gives rise to identical $\tilde{c}_{\rm eff}$ as the energy defect. Recall that the same was also observed for $c_{\rm eff}$ during the computation of the interface EE (see also figure 7). This can be viewed as a consequence of the fact that the microscopic Hamiltonians for the two kinds of defects are essentially identical barring the zero energy modes for the duality defect. This is clearly visible in the fermionic formulation (see section 2). However, as for the EE, the zero energy modes give rise to two distinct effects. First, they affect the subleading term, $\tilde{\mathcal{E}}_0$ in eq. (4.1). This manifests itself in a difference between the offsets for energy and duality defects for a given defect strength [see figure 6, infinite bc and $l \ll L$ part of the open bc]. Interestingly, the subleading term is *lower* for the duality defect compared to the energy defect for the same defect strength. This is in contrast to the symmetric and interface EEs, where the subleading term was higher for the duality defect. In fact, the higher symmetric EE due to the unpaired zero mode within the interval A is directly related to the lower log-EN between B_1 and B_2. Intuitively, the enhanced EE of A must be accompanied by a lowering of entanglement between B_1 and B_2 since the system overall remains in a pure state. Second, the local and nonlocal zero modes of the duality defect give rise to finite-size corrections to the log-EN, similar to what is described for the EE in section 3.2. This is visible in the deviations from the logarithmic scaling the log-EN for the open bc (figure 6, right panel, $l \sim L$). Notice there is no such effect for the energy defect with open bc since

JHEP06(2022)165

the latter has no zero modes. Figure 7 summarizes the results for the effective central charges and offsets computed for the interface EE and log-EN.

5 Conclusion and outlook

To summarize, we analyzed the rich entanglement properties of the Ising CFT in the presence of defects. In particular, we computed the EEs (symmetric and interface) and the log-EN for subsystems in the presence of energy and duality defects using DMRG. We showed that for the duality defect, due to the existence of zero energy modes, the EEs and the log-EN respectively receive positive and negative additional contributions compared to the energy defect of the same defect strength. For finite systems, the same zero energy modes also give rise to finite-size corrections for both the EE and the log-EN, which lead to deviations from the usual logarithmic scaling that is characteristic of one-dimensional critical systems.

Before concluding, we present some potential future directions of research. First, we computed the log-EN numerically using DMRG for the case with defects. In the absence of defects, the log-EN can be computed using replica techniques for CFTs [60–62]. Potentially, the existing computations of the interface EE [41, 42] can be generalized to compute the leading term of the logarithmic scaling of the log-EN. The computations of the subleading term for the log-EN and the associated finite-size corrections due to the zero energy modes remain also open problems, which are likely beyond the scope of the aforementioned computation. Second, in this work, we have focussed on the EE and the log-EN as entanglement measures for the defect setting. Yet another quantity of particular significance is the entanglement or modular Hamiltonian [66]. The latter plays a central role in the analysis of topological phases of matter in 2+1 space-time dimensions [67]. For 1+1D CFTs, the spectra of the entanglement Hamiltonians can be related to the Hamiltonian spectra of corresponding boundary CFTs [20, 21, 68]. It will be interesting to generalize these results to the case of defects. We note that some progress has been made for massless Dirac fermions [69] and the chiral fermions with zero modes (equivalently the antiperiodic Ising chain) [47]. Third, in recent works, the concept of entanglement Hamiltonian, which is typically written for the total system being in pure state, has been generalized to the case when the total system is mixed. This leads to the concept of negativity Hamiltonian [70, 71]. It is an interesting open problem to consider generalizations of these concepts to the cases with defects. Fourth, we note that defect Hamiltonians for other rational CFTs contain more complicated set of zero modes [24]. The question of subleading corrections in the EEs for these models remains open. Finally, the zero modes in the Ising model with the duality defects are reminiscent of the zero modes of gapless symmetry-protected-topological phases [72]. It will be interesting to further analyze this relationship. We hope to return to some of these questions in the future.

Note added in proof. After the completion of the paper, the authors became aware of the fact that the values of $\tilde{c}_{\text{eff}}$ shown in figure 7 are in excellent agreement with the results of refs. [79, 82]. The latter works analyze a different geometric configuration, that of two segments connected through a conformal defect. We are grateful to Viktor Eisler for bringing this to our attention.

JHEP06(2022)165

Acknowledgments

AR acknowledges discussions with Hubert Saleur and Johannes Hauschild. AR was supported from a grant from the Simons Foundation (825876, TDN). FP acknowledges support of the European Research Council (ERC) under the European Unions Horizon 2020 research and innovation program (grant agreement No. 771537). FP also acknowledges the support of the Deutsche Forschungsgemeinschaft (DFG, German Research Foundation) under Germany's Excellence Strategy EXC-2111-390814868. FP's research is part of the Munich Quantum Valley, which is supported by the Bavarian state government with funds from the Hightech Agenda Bayern Plus.

A Computation of symmetric entanglement entropy and negativity with matrix product states

Density Matrix Renormalization Group (DMRG) calculations use the fact that ground states of a local 1D lattice Hamiltonian can be efficiently represented by Matrix Product States (MPS). Such a state $|\Psi\rangle$ is nicely visualized in Penrose tensor notation as

$|\Psi\rangle =$ 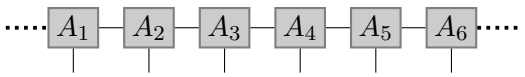

. (A.1)

Each box is a tensor of rank equal to the number of legs connected to it. In this example, all tensors are of rank 3. The unconnected lose legs represent the physical dimension D which is in the case of Spin-$\frac{1}{2}$ Systems $D = 2$. The horizontal virtual bonds are of dimension χ, the bond dimension. The bond dimension is a controllable parameter directly governing the entanglement captured by the MPS.

In the following we assume that $|\Psi\rangle$ is in left canonical form such that

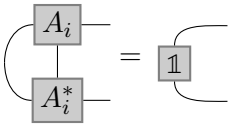

(A.2)

and

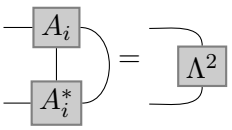

. (A.3)

Λ is a diagonal matrix carrying the Schmidt values of a bipartition on that bond. This efficient tensor network representation can be used to construct reduced density operators in an economical way [73, 74]. Using the formal definition of the density operator

$$\hat{\rho} = |\Psi\rangle\langle\Psi| \tag{A.4}$$

JHEP06(2022)165

for matrix product states gives

$\hat{\rho} =$ 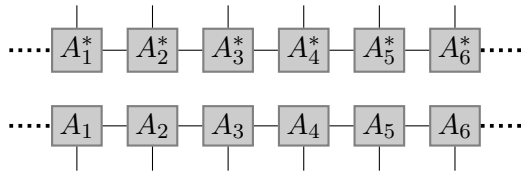 (A.5)

the so-called matrix product density operator. As each tensor represent a specific lattice site, different system partitions can be applied to the operator.

The Symmetric Entanglement entropy is obtained by assigning a central segment to subsystem A (red) and the rest to subsystem B (blue):

$\hat{\rho} =$ 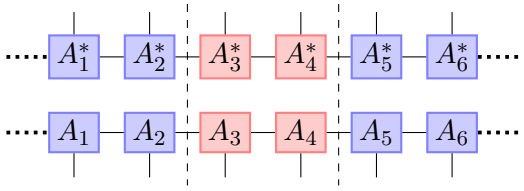 . (A.6)

After tracing over the subsystem A

$\mathrm{Tr}_A\,\hat{\rho} =$ 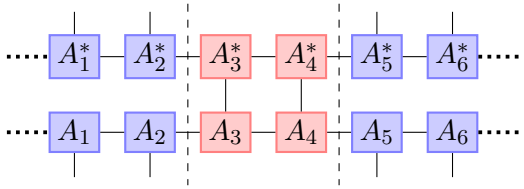 (A.7)

the center can be represented very similar to a transfer matrix T_A

$\mathrm{Tr}_A\,\hat{\rho} =$ 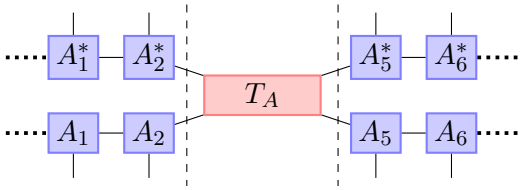 . (A.8)

The possibly infinite segments of subsystem B can be compressed without any losses by using the properties of the canonical form. This can be understood by first tracing over each half of B as well:

$\tilde{\mathrm{Tr}}_A\hat{\rho} =$ 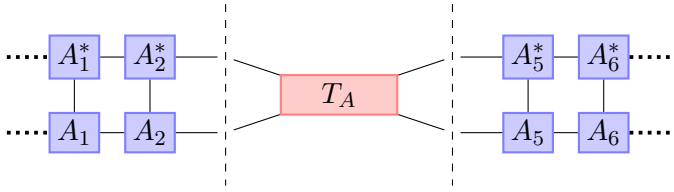 (A.9)

Due to the canonical form this simplifies to

$\tilde{\mathrm{Tr}}_A\hat{\rho} =$ 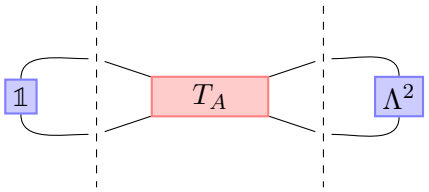 . (A.10)

JHEP06(2022)165

After splitting the outside matrices by matrix factorizing the compressed form of the reduced density matrix is

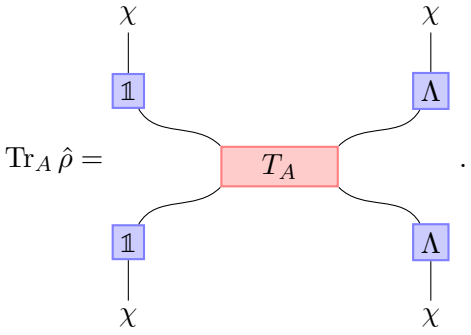

(A.11)

As DMRG already gives access to the Schmidt values Λ at each bond, only the contraction of T_A must be performed. This scales with $O(\chi^5)$ in computational complexity and $O(\chi^4)$ in memory. The final operator is of dimension χ^4 independent of the number of lattice sites involved. This is in contrast to a naive construction. If the tensor network structure of the state is neglected the matrix will scale exponentially in memory with D^{2l} where l is the segment size. We want to emphasize that no additional approximations apart from the finite bond dimensions of the DMRG calculations were performed. A nearly identical method can be used to calculate the negativity of two segments touching the possibly infinite boundaries separated by a finite interval. The segmentation used in this case is

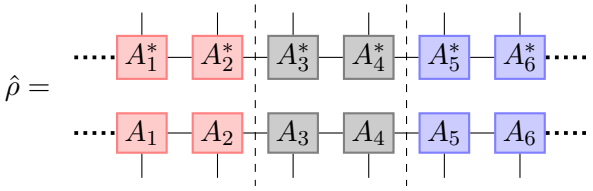

(A.12)

where segment B_1 is shown in red, segment B_2 in blue and the separating gap A in gray. After following analogous steps to the above, this results in

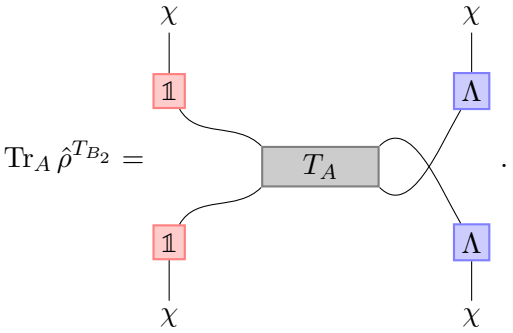

(A.13)

After tracing over the separating interval the individual subsystems are still individually accessible. This allows to partially transpose segment B_2 by twisting the corresponding legs.

JHEP06(2022)165

References

[1] A. Roy and H. Saleur, *Entanglement Entropy in the Ising Model with Topological Defects*, *Phys. Rev. Lett.* **128** (2022) 090603 [arXiv:2111.04534] [INSPIRE].

[2] C. Holzhey, F. Larsen and F. Wilczek, *Geometric and renormalized entropy in conformal field theory*, *Nucl. Phys. B* **424** (1994) 443 [hep-th/9403108] [INSPIRE].

[3] P. Calabrese and J. Cardy, *Entanglement entropy and quantum field theory*, *J. Stat. Mech.* **2004** (2004) P06002 [hep-th/0405152] [INSPIRE].

[4] H. Casini, *Geometric entropy, area, and strong subadditivity*, *Class. Quant. Grav.* **21** (2004) 2351 [hep-th/0312238] [INSPIRE].

[5] H. Casini and M. Huerta, *A c-theorem for the entanglement entropy*, *J. Phys. A* **40** (2007) 7031 [cond-mat/0610375] [INSPIRE].

[6] A.B. Zamolodchikov, *Irreversibility of the Flux of the Renormalization Group in a 2D Field Theory*, *JETP Lett.* **43** (1986) 730 [INSPIRE].

[7] P. Calabrese and A. Lefevre, *Entanglement spectrum in one-dimensional systems*, *Phys. Rev. A* **78** (2008) 032329 [arXiv:0806.3059].

[8] L. Tagliacozzo, T.R. de Oliveira, S. Iblisdir and J.I. Latorre, *Scaling of entanglement support for Matrix Product States*, *Phys. Rev. B* **78** (2008) 024410 [arXiv:0712.1976] [INSPIRE].

[9] F. Pollmann, S. Mukerjee, A.M. Turner and J.E. Moore, *Theory of finite-entanglement scaling at one-dimensional quantum critical points*, *Phys. Rev. Lett.* **102** (2009) 255701 [arXiv:0812.2903].

[10] M.B. Hastings, *An area law for one-dimensional quantum systems*, *J. Stat. Mech.* **08** (2007) P08024 [arXiv:0705.2024] [INSPIRE].

[11] S.R. White, *Density matrix formulation for quantum renormalization groups*, *Phys. Rev. Lett.* **69** (1992) 2863 [INSPIRE].

[12] U. Schollwöck, *The density-matrix renormalization group in the age of matrix product states*, *Annals Phys.* **326** (2011) 96 [arXiv:1008.3477].

[13] A. Roy and H. Saleur, *Entanglement entropy in critical quantum spin chains with boundaries and defects*, arXiv:2111.07927 [INSPIRE].

[14] I. Affleck and A.W.W. Ludwig, *Universal noninteger 'ground state degeneracy' in critical quantum systems*, *Phys. Rev. Lett.* **67** (1991) 161 [INSPIRE].

[15] P. Calabrese and J. Cardy, *Entanglement entropy and conformal field theory*, *J. Phys. A* **42** (2009) 504005 [arXiv:0905.4013] [INSPIRE].

[16] I. Affleck, *Conformal field theory approach to the Kondo effect*, *Acta Phys. Polon. B* **26** (1995) 1869 [cond-mat/9512099] [INSPIRE].

[17] H. Saleur, *Lectures on nonperturbative field theory and quantum impurity problems*, cond-mat/9812110 [INSPIRE].

[18] M.R. Gaberdiel, *Lectures on nonBPS Dirichlet branes*, *Class. Quant. Grav.* **17** (2000) 3483 [hep-th/0005029] [INSPIRE].

[19] I. Affleck, N. Laflorencie and E.S. Sørensen, *Entanglement entropy in quantum impurity systems and systems with boundaries*, *J. Phys. A* **42** (2009) 504009 [arXiv:0906.1809] [INSPIRE].

JHEP06(2022)165

[20] J. Cardy and E. Tonni, *Entanglement hamiltonians in two-dimensional conformal field theory*, *J. Stat. Mech.* **2016** (2016) 123103 [arXiv:1608.01283] [INSPIRE].

[21] A. Roy, F. Pollmann and H. Saleur, *Entanglement Hamiltonian of the 1+1-dimensional free, compactified boson conformal field theory*, *J. Stat. Mech.* **2008** (2020) 083104 [arXiv:2004.14370] [INSPIRE].

[22] J.L. Cardy, *Boundary Conditions, Fusion Rules and the Verlinde Formula*, *Nucl. Phys. B* **324** (1989) 581 [INSPIRE].

[23] J. Belletête, A.M. Gainutdinov, J.L. Jacobsen, H. Saleur and T.S. Tavares, *Topological defects in lattice models and affine Temperley-Lieb algebra*, arXiv:1811.02551 [INSPIRE].

[24] J. Belletête, A.M. Gainutdinov, J.L. Jacobsen, H. Saleur and T.S. Tavares, *Topological defects in periodic RSOS models and anyonic chains*, arXiv:2003.11293.

[25] D. Aasen, P. Fendley and R.S.K. Mong, *Topological defects on the lattice: Dualities and degeneracies*, arXiv:2008.08598 [INSPIRE].

[26] M. Henkel, A. Patkos and M. Schlottmann, *The Ising Quantum Chain With Defects. 1. The Exact Solution*, *Nucl. Phys. B* **314** (1989) 609 [INSPIRE].

[27] M. Baake, P. Chaselon and M. Schlottmann, *The Ising Quantum Chain With Defects. 2. The SO(2n) Kac-Moody Spectra*, *Nucl. Phys. B* **314** (1989) 625 [INSPIRE].

[28] U. Grimm, *The Quantum Ising Chain With a Generalized Defect*, *Nucl. Phys. B* **340** (1990) 633 [hep-th/0310089] [INSPIRE].

[29] M. Oshikawa and I. Affleck, *Boundary conformal field theory approach to the critical two-dimensional Ising model with a defect line*, *Nucl. Phys. B* **495** (1997) 533 [cond-mat/9612187] [INSPIRE].

[30] U. Grimm, *Spectrum of a duality twisted Ising quantum chain*, *J. Phys. A* **35** (2002) L25 [hep-th/0111157] [INSPIRE].

[31] V.B. Petkova and J.B. Zuber, *Generalized twisted partition functions*, *Phys. Lett. B* **504** (2001) 157 [hep-th/0011021] [INSPIRE].

[32] C. Bachas, J. de Boer, R. Dijkgraaf and H. Ooguri, *Permeable conformal walls and holography*, *JHEP* **06** (2002) 027 [hep-th/0111210] [INSPIRE].

[33] J. Fröhlich, J. Fuchs, I. Runkel and C. Schweigert, *Kramers-Wannier duality from conformal defects*, *Phys. Rev. Lett.* **93** (2004) 070601 [cond-mat/0404051] [INSPIRE].

[34] J. Fröhlich, J. Fuchs, I. Runkel and C. Schweigert, *Duality and defects in rational conformal field theory*, *Nucl. Phys. B* **763** (2007) 354 [hep-th/0607247] [INSPIRE].

[35] D. Aasen, R.S.K. Mong and P. Fendley, *Topological Defects on the Lattice I: The Ising model*, *J. Phys. A* **49** (2016) 354001 [arXiv:1601.07185] [INSPIRE].

[36] H.A. Kramers and G.H. Wannier, *Statistics of the two-dimensional ferromagnet. Part 1*, *Phys. Rev.* **60** (1941) 252 [INSPIRE].

[37] R. Savit, *Duality in Field Theory and Statistical Systems*, *Rev. Mod. Phys.* **52** (1980) 453 [INSPIRE].

[38] M. Buican and A. Gromov, *Anyonic Chains, Topological Defects, and Conformal Field Theory*, *Commun. Math. Phys.* **356** (2017) 1017 [arXiv:1701.02800] [INSPIRE].

JHEP06(2022)165

[39] H. Saleur, *Lectures on nonperturbative field theory and quantum impurity problems: Part 2*, cond-mat/0007309 [INSPIRE].

[40] M. Gutperle and J.D. Miller, *A note on entanglement entropy for topological interfaces in RCFTs*, *JHEP* **04** (2016) 176 [arXiv:1512.07241] [INSPIRE].

[41] K. Sakai and Y. Satoh, *Entanglement through conformal interfaces*, *JHEP* **12** (2008) 001 [arXiv:0809.4548] [INSPIRE].

[42] E.M. Brehm and I. Brunner, *Entanglement entropy through conformal interfaces in the 2D Ising model*, *JHEP* **09** (2015) 080 [arXiv:1505.02647] [INSPIRE].

[43] V. Eisler and I. Peschel, *Entanglement in fermionic chains with interface defects*,*Annalen Phys.* **522** (2010) 679.

[44] I. Peschel and V. Eisler, *Exact results for the entanglement across defects in critical chains*, *J. Phys. A* **45** (2012) 155301 [arXiv:1201.4104].

[45] P. Calabrese, M. Mintchev and E. Vicari, *Entanglement Entropy of Quantum Wire Junctions*, *J. Phys. A* **45** (2012) 105206 [arXiv:1110.5713] [INSPIRE].

[46] J. Hauschild and F. Pollmann, *Efficient numerical simulations with Tensor Networks: Tensor Network Python (TeNPy)*, *SciPost Phys. Lect. Notes* **2018** (2018) 5 [arXiv:1805.00055].

[47] I. Klich, D. Vaman and G. Wong, *Entanglement Hamiltonians for chiral fermions with zero modes*, *Phys. Rev. Lett.* **119** (2017) 120401 [arXiv:1501.00482] [INSPIRE].

[48] G. Vidal and R.F. Werner, *Computable measure of entanglement*, *Phys. Rev. A* **65** (2002) 032314 [quant-ph/0102117] [INSPIRE].

[49] F. Iglói and I. Peschel, *On reduced density matrices for disjoint subsystems*, *Europhys. Lett.* **89** (2010) 40001 [arXiv:0910.5671].

[50] L.P. Kadanoff and H. Ceva, *Determination of an opeator algebra for the two-dimensional Ising model*, *Phys. Rev. B* **3** (1971) 3918 [INSPIRE].

[51] J.L. Cardy, *Continuously varying exponents and the value of the central charge*, *J. Phys. A* **20** (1987) L891.

[52] F. Iglói, I. Peschel and L. Turban, *Inhomogeneous systems with unusual critical behaviour*, *Adv. Phys.* **42** (1993) 683 [cond-mat/9312077].

[53] U. Grimm and G.M. Schutz, *The Spin 1/2 XXZ Heisenberg chain, the quantum algebra U(q)[sl(2)], and duality transformations for minimal models*, *J. Statist. Phys.* **71** (1993) 921 [hep-th/0111083] [INSPIRE].

[54] J.L. Cardy, *Finite-size scaling in strips: antiperiodic boundary conditions*, *J. Phys. A* **17** (1984) L961.

[55] C.P. Herzog and T. Nishioka, *Entanglement Entropy of a Massive Fermion on a Torus*, *JHEP* **03** (2013) 077 [arXiv:1301.0336] [INSPIRE].

[56] C. Bachas, I. Brunner and D. Roggenkamp, *Fusion of Critical Defect Lines in the 2D Ising Model*, *J. Stat. Mech.* **1308** (2013) P08008 [arXiv:1303.3616] [INSPIRE].

[57] L. Lewin, *Polylogarithms and associated functions*, North Holland, Amsterdam, The Netherlands (1981).

[58] L. Amico, R. Fazio, A. Osterloh and V. Vedral, *Entanglement in many-body systems*, *Rev. Mod. Phys.* **80** (2008) 517 [quant-ph/0703044] [INSPIRE].

JHEP06(2022)165

[59] R. Horodecki, P. Horodecki, M. Horodecki and K. Horodecki, *Quantum entanglement*, *Rev. Mod. Phys.* **81** (2009) 865 [quant-ph/0702225] [INSPIRE].

[60] P. Calabrese, J. Cardy and E. Tonni, *Entanglement negativity in quantum field theory*, *Phys. Rev. Lett.* **109** (2012) 130502 [arXiv:1206.3092] [INSPIRE].

[61] P. Calabrese, J. Cardy and E. Tonni, *Entanglement negativity in extended systems: a field theoretical approach*, *J. Stat. Mech.* **2013** (2013) P02008 [arXiv:1210.5359] [INSPIRE].

[62] P. Calabrese, L. Tagliacozzo and E. Tonni, *Entanglement negativity in the critical Ising chain*, *J. Stat. Mech.* **1305** (2013) P05002 [arXiv:1302.1113] [INSPIRE].

[63] O. Blondeau-Fournier, O.A. Castro-Alvaredo and B. Doyon, *Universal scaling of the logarithmic negativity in massive quantum field theory*, *J. Phys. A* **49** (2016) 125401 [arXiv:1508.04026] [INSPIRE].

[64] M. Hoogeveen and B. Doyon, *Entanglement negativity and entropy in non-equilibrium conformal field theory*, *Nucl. Phys. B* **898** (2015) 78 [arXiv:1412.7568] [INSPIRE].

[65] V. Eisler and Z. Zimborás, *Entanglement negativity in the harmonic chain out of equilibrium*, *New J. Phys.* **16** (2014) 123020 [arXiv:1406.5474].

[66] R. Haag, *Local Quantum Physics: Fields, Particles, Algebras*, *Theoretical and Mathematical Physics*, Springer, Heidelberg, Germany (2012).

[67] H. Li and F. Haldane, *Entanglement Spectrum as a Generalization of Entanglement Entropy: Identification of Topological Order in Non-Abelian Fractional Quantum Hall Effect States*, *Phys. Rev. Lett.* **101** (2008) 010504 [arXiv:0805.0332] [INSPIRE].

[68] V. Alba, P. Calabrese and E. Tonni, *Entanglement spectrum degeneracy and the Cardy formula in 1+1 dimensional conformal field theories*, *J. Phys. A* **51** (2018) 024001 [arXiv:1707.07532] [INSPIRE].

[69] M. Mintchev and E. Tonni, *Modular Hamiltonians for the massless Dirac field in the presence of a defect*, *JHEP* **03** (2021) 205 [arXiv:2012.01366] [INSPIRE].

[70] P. Ruggiero, V. Alba and P. Calabrese, *Negativity spectrum of one-dimensional conformal field theories*, *Phys. Rev. B* **94** (2016) 195121 [arXiv:1607.02992] [INSPIRE].

[71] S. Murciano, V. Vitale, M. Dalmonte and P. Calabrese, *Negativity Hamiltonian: An Operator Characterization of Mixed-State Entanglement*, *Phys. Rev. Lett.* **128** (2022) 140502 [arXiv:2201.03989] [INSPIRE].

[72] R. Verresen, N.G. Jones and F. Pollmann, *Topology and Edge Modes in Quantum Critical Chains*, *Phys. Rev. Lett.* **120** (2018) 057001 [arXiv:1709.03508] [INSPIRE].

[73] P. Ruggiero, V. Alba and P. Calabrese, *Entanglement negativity in random spin chains*, *Phys. Rev. B* **94** (2016) 035152 [arXiv:1605.00674] [INSPIRE].

[74] H. Wichterich, J. Molina-Vilaplana and S. Bose, *Scaling of entanglement between separated blocks in spin chains at criticality*, *Phys. Rev. A* **80** (2009) 010304 [arXiv:0811.1285] [INSPIRE].

[75] R.Z. Bariev, *Effect of Linear Defects on the Local Magnetization of a Plane Ising Lattice*, *JETP* **50** (1979) 613.

[76] A. Bayat, P. Sodano and S. Bose, *Negativity as the Entanglement Measure to Probe the Kondo Regime in the Spin-Chain Kondo Model*, *Phys. Rev. B* **81** (2010) 064429 [arXiv:0904.3341] [INSPIRE].

JHEP06(2022)165

[77] A. Bayat, S. Bose, P. Sodano and H. Johannesson, *Entanglement probe of two-impurity Kondo physics in a spin chain*, *Phys. Rev. Lett.* **109** (2012) 066403 [arXiv:1201.6668] [INSPIRE].

[78] B. Alkurtass, *Entanglement Structure of the Two-Channel Kondo Model*, *Phys. Rev. B* **93** (2016) 081106 [arXiv:1509.02949].

[79] M. Gruber and V. Eisler, *Time evolution of entanglement negativity across a defect*, *J. Phys. A* **53** (2020) 205301 [arXiv:2001.06274] [INSPIRE].

[80] L.-F. Ko, H. Au-Yang and J.H.H. Perk, *Energy-Density Correlation Functions in the Two-Dimensional Ising Model with a Line Defect*, *Phys. Rev. Lett.* **54** (1985) 1091.

[81] B.M. McCoy and J.H.H. Perk, *Two Spin Correlation Functions of an Ising Model With Continuous Exponents*, *Phys. Rev. Lett.* **44** (1980) 840 [INSPIRE].

[82] I. Peschel and V. Eisler, *Exact Results for the Entanglement across Defects in Critical Chains*, *J. Phys. A* **45** (2012) 155301 [arXiv:1201.4104].

JHEP06(2022)165